Effect of test setup on the fiber-to-mortar pull-out response in TRM composites Experimental and analytical modeling

Dalalbashi, Ali; Ghiassi, Bahman; Oliveira, Daniel V.; Freitas, Ana

DOI
10.1016/j.compositesb.2018.02.010

Publication date
2018

Document Version
Accepted author manuscript

Published in
Composites Part B: Engineering

Effect of test setup on the fiber-to-mortar pull-out response in TRM composites: experimental and analytical modeling

Ali Dalalbashi[1], Bahman Ghiassi[2], Daniel V. Oliveira[3], Ana Freitas[4]

ABSTRACT

Textile-reinforced mortars (TRM) have recently received significant attention for the externally bonded reinforcement (EBR) of masonry and historical structures. The fiber-to-mortar bond, the TRM-to-masonry bond, and the mechanical properties of the TRM constituents have a fundamental role in the performance of this strengthening technique and therefore require special attention. Despite this importance, only few investigations are devoted to characterization of the single fiber-to-mortar bond response in these systems.

This paper, as an step towards addressing the fiber-to-mortar bond, presents a combined experimental and analytical investigation on the effect of test setup on the pull-out response and bond-slip laws in TRM composites. Three different pull-out test setups, consisting of one pull-pull and two pull-push configurations, are developed and investigated for characterization of the single fiber-to-mortar bond behavior. The experimental and analytical results are critically discussed and presented and bond-slip laws are extracted for each test setup.

Keywords: Fiber/matrix bond; Mechanical testing; Analytical modeling; Textile-reinforced mortar (TRM)

---

[1] PhD Student, ISISE, University of Minho, Department of Civil Engineering, Azurém, 4800-058 Guimarães, Portugal. Phone: +351 253 510 499, fax: +351 253 510 217, E-mail: alidalalbashi@gmail.com
[2] Marie Curie IF Research Associate, Department of Civil Engineering and Geosciences, TU Delft, Delft, The Netherlands. Phone: +31 15 2788741, E-mail: bahmanghiassi@gmail.com
[3] Associate Professor, ISISE, University of Minho, Department of Civil Engineering, Azurém, 4800-058 Guimarães, Portugal. Phone: +351 253 510 200, fax: +351 253 510 217, E-mail: danvco@civil.uminho.pt
[4] Master Student, University of Minho, Department of Civil Engineering, Azurém, 4800-058 Guimarães, Portugal. Phone: +351 253 510 499, fax: +351 253 510 217, E-mail: a65198@alumni.uminho.pt

1 Introduction

Textile reinforced mortars (TRMs) have recently received an extensive attention for externally bonded reinforcement (EBR) of masonry and historical structures. In comparison to fiber reinforced polymer composites (FRPs), TRMs exhibit several advantages such as fire resistance, vapor permeability, removability, and compatibility with the substrate [1–5]. TRMs are composed of continuous fibers embedded in an inorganic matrix that is applied to the surface of the structure on site. The available textile fibers are diverse and consist of steel, glass and basalt fibers, to name a few. As for the matrix, cementitious or lime-based mortars are usually used. Lime-based mortars are preferred for application to masonry and historical structures due to their compatibility, sustainability, breathability and capability to accommodate structural movements [6–8].

The mechanical properties of TRM composites and their effectiveness in improving the performance of masonry structures are strongly dependent on the mortar and fiber properties, the bond at the fiber-to-mortar interface and the bond at the TRM-to-masonry interface [9]. While several studies can be found in the literature devoted to characterization of mechanical properties of TRMs, e.g. [10–12], or to the characterization of TRM-to-masonry bond behavior, e.g. [3,13], the fiber-to-mortar bond response in these systems has only received a limited attention [9]. This mechanism is however critical for fully utilization of this strengthening system and, without any doubt, requires special attention [9].

Although there is a gap in literature on fiber-to-mortar bond response in TRM composites (made of lime-based mortars), several information can be found regarding this mechanism

in textile reinforced concrete (TRC), where cementitious mortars are utilized [14]. The available results show that the mechanical properties of the textile and the mortar, the chemical interaction between them [14–18] as well as the fiber embedded length [19,20] and orientation with respect to the crack surface [21–23] are among the main parameters that can affect the fiber-to-mortar bond response. A variety of pull-out test setups have been used in literature for the characterization of the fiber-to-mortar (or concrete) bond behavior. These can generally be categorized into pull-push (or single-sided) [24–26] and pull-pull (or double-sided) [27,28] tests. However, the differences between the experimental results obtained from different test setups are poorly addressed.

Among the few available studies on the characterization of fiber-to-mortar bond behavior of TRM-strengthened masonry, Ghiassi et al. [9] used a single-sided pull-out test configuration on fibers embedded in cylindrical specimens. They, however, reported difficulties in preparation of the specimens (vertical alignment of the fibers) and in measurement of the slip during the tests due to the flexibility of the fibers. Additionally, due to the geometrical limitations of the test setup, the LVDTs used for slip measurements were attached at a certain distance from the mortar edge. The elastic deformation of the fibers therefore had to be reduced from the recorded values with the LVDTs that could lead to additional uncertainty in the slip measurements.

The present study, as an attempt for development of an optimized test setup for performing the pull-out tests, presents a combined experimental, analytical and numerical investigation on the effect of test setup and configuration on the pullout respose of TRM composites. Three test setups consisting of two pull-push and one pull-pull configurations are developed to perform the pull-out tests. Steel fiber embedded in a pozzolanic lime-based

mortar (also referred as SRG in the literature) is used as a conventional composite material for strengthening of masonry structures. The experimental results are compared and critically discussed in terms of force-slip response, stiffness, toughness and peak load. With the aim of analytical and numerical modeling, bond-slip laws are also extracted from the experimental results obtained from each test setup and the results are compared.

2 Experimental Program

The experimental program consists of a series of pull-out tests on the specimens tested in three different test setups. The detailed procedure followed for preparation of the specimens and performing the tests are given in this section.

2.1 Materials

Materials consist of a commercially available hydraulic lime-based mortar as the matrix and a commercially available steel fiber as the reinforcing material. Based on the technical sheets provided by the manufacturer, the compressive strength and elastic modulus of the mortar after 28 days are 15 MPa and 9.23 GPa, respectively. The mortar is prepared according to the manufacturer's technical sheets by mixing 0.204 liter of water with 1 kg of powder. A low-speed mechanical mixer is used to mix the paste for seven minutes until the blend is completely homogeneous and no powder is remained in the container. The reinforcing material is a unidirectional ultra-high tensile strength steel fiber, with a density of 670 g/m^2, an effective area and equivalent diameter of one cord (five filaments) equal to 0.538 mm^2 and 0.827 mm, respectively, a tensile strength of 2820 MPa, and an elastic modulus of 190 GPa according to the technical datasheets provided by the manufacturer.

2.2 Material characterization tests

For mechanical characterization of the mortar, compressive and flexural tests are performed according to ASTM C109 [29] and EN 1015-11 [30] at different ages. Five cubic ($50\times50\times50$ mm^3) and five prismatic ($40\times40\times160$ mm^3) specimens are prepared for compressive and flexural tests at each age, respectively. The tests are carried out with a Lloyd testing machine under force-controlled conditions at a rate of 2.5 N/s (for the compressive tests) and 10 N/s (for the flexural tests), as shown in Fig. 1. In the compressive tests, for reducing the friction at the specimens' boundaries and ensuring a uniform distribution of stresses at the center of the specimens, a pair of friction-reducing Teflon sheets with a layer of oil in between is placed between the specimens and the compression plates (Fig. 1a). The flexural tests are performed according to the three-point bending test scheme with a 100 mm distance between the supports (Fig. 1b).

As for the steel fibers, direct tensile tests are conducted [3,9] to obtain their tensile strength and elastic modulus. A universal testing machine with a maximum load capacity of 10 kN is used for these tests. The tests are performed under displacement-controlled conditions at the rate of 0.3 mm/min (Fig. 1c). The free length of specimens is 300 mm. A 100 mm clip gauge is attached to the center of the specimens to measure the fiber strain during the tests.

2.3 Bond characterization tests

In the pull-push tests, the mortar is fixed from the top and the fiber is pulled out from the same direction. Compressive stresses are therefore generated in the mortar near the loaded end in this test configuration. In the pull-pull tests, on the other hand, the mortar is fixed from the bottom and the fiber is pulled out from the top (or vice versa) simulating direct tensile tests. Tensile stresses are therefore developed in the mortar in this test setup. Due to

the different stress conditions imposed on the specimens in these test configurations, different pull-out responses are therefore expected.

Two pull-push and one pull-pull test setups are used in this study for performing the pull-out tests. Five specimens are prepared and tested for each test setup (see Table 1 for information). Based on the previous studies performed by the authors, the bonded length is selected as 150 mm to be larger than the effective bond length.

The first pull-push test setup (pull-push I) is the one used by Ghiassi et al. [9]. In these tests, the specimens are made of fibers embedded in mortar cylinders with a 150 mm bonded length and a 150 mm free length for gripping. The preparation of the specimens is performed following the procedure detailed in Ghiassi et al. [9]: (1) cleaning the fibers; (2) adjusting the PVC mold on the base; (3) placing the cleaned fibers in the center of the mold; (4) applying a first layer of mortar until half of the mold height; (5) tamping the mortar; and (6) pouring the second layer of mortar. Diameter and height of specimens are 75 mm and 150 mm, respectively. Two steel plates are attached to the end of the fibers 48 hours before the test day to facilitate gripping during the tests (Fig. 2a and Fig. 3a). For performing the tests, a supporting frame is placed on top of the mortar cylinders and is fixed from the bottom to a rigid steel frame to avoid movements of the specimens during the tests. An LVDT is attached to the fiber at 6.3 mm distance from the mortar edge to measure the fiber slip during the tests. It is therefore necessary to reduce the elastic deformation of the fiber along this 6.3 mm from the measured experimental values to obtain the fiber slip.

The second pull-push test setup (pull-push II) is designed to mitigate the problems related to slip measurements in pull-push I test setup. The sample's geometry, the supporting

system, and the gripping methods are therefore changed accordingly. In this test setup, the mortar prepared in a disk shape with the dimensions of 150×125×16 mm^3 to facilitate preparation of the specimens and alignment of the fiber inside the mortar. The free length of the fiber is also embedded in an epoxy resin block over a length of 200 mm and with a rectangular cross-sectional area of 10×16 mm^2. This block offers protection against early and uncontrolled failure caused by clamping and at the same time facilitates slip measurements during the tests (Fig. 2b and Fig. 3b). This technique was first proposed by Banholzer [31]. The preparation of the specimens is as follows: (1) embedment of the fiber free length in epoxy resin and curing for 48 hours (Fig. 4a); (2) preparation and cleaning of the mold and the fiber; (2) applying a first layer of mortar with a thickness of 8 mm inside the molds (Fig. 4b); (3) placing the fiber on top of the first mortar layer; (4) applying a second layer of mortar with a thickness of 8 mm (Fig. 4c). The specimens are tested in a similar test configuration as of pull-push I test setup. However, a U-shape steel support is used here for supporting the specimens as shown in Fig. 2b and Fig. 3b. A mechanical clamp is used to grip the epoxy resin (and thus the fiber) from the top and performing the tests. Two LVDTs with 20 mm range and 2-µm sensibility are located at both sides of the epoxy block to record the slip. The average of these LVDTs measurements are presented as the slip in the experimental results.

In the third test setup type (pull-pull), specimens have a similar geometry to the pull-push II test setup, but the supporting system is different. In this test setup, the specimens are gripped from the bottom thus simulating tensile tests. The specimens are prepared following the same procedure as pull-push II tests. The specimens are slightly longer in this case, the mortar disks are with dimensions of 250×125×16 mm^3 to provide additional space

for gripping from the bottom. To prevent crushing of the mortar in the gripping area during the tests, the lower part of the specimens is reinforced by placing additional steel fibers as shown in Fig. 2c. A mechanical clamp is used to grip the epoxy resin (and thus the fiber) from the top and another one to grip the mortar from the bottom (Fig. 3c). The LVDTs are placed at similar locations as in the pull-push II tests.

Based on a literature review [6,7,30,32,33], specimens are demolded after 24 hours of preparation and are placed in a damp environment for seven days. After that, specimens are stored in the lab environmental conditions (20°C, 60% RH) until the test day (for 60 days of mortar curing).

All the tests are carried out using a servo-hydraulic system with a maximum capacity of 25 kN at a displacement rate of 1.0 mm/min.

3 Experimental results and discussion

3.1 Material properties

The mean compressive and flexural strength of the mortar at different ages are presented in Table 2 and Fig. 5. As illustrated, the strength of the mortar increases significantly in the first 30 days and, besides some variations, the changes are not significant after that, particularly for the compressive strength. The maximum compressive and flexural strength of the mortar are 9.53 MPa and 2.54 MPa, respectively. The average tensile strength and Young's modulus of the steel fiber are 3141 MPa and 174.87 GPa, respectively.

3.2 Effect of test setup

The envelope and average of the load-slip curves obtained from each test setup are illustrated in Fig. 6. The force-slip curves from different test setups are generally similar

with some differences in the peak load, the initial stiffness and consequently the toughness. These parameters are the main outcomes of the pull-out tests that are used for investigation of the bond behavior [26,34] and can significantly affect the experimental interpretations or the extracted bond-slip laws.

The peak load and its corresponding slip are directly obtained from the experimental force-slip curves. The initial stiffness is obtained as the slope of the linear portion of the force-slip curve and corresponds to the initial stage of the stress transfer before occurrence of any interfacial cracking [9,26,34]. The toughness or absorbed energy is defined as the area under the force-slip curve [20,26,34–36]. The bond between the fiber and the mortar has a significant influence on the fiber ability to stabilize crack propagation in the mortar and consequently on the total energy consumption. Here, as also suggested in the literature [25,37], the area under the force-slip curve until the peak load is considered as the toughness or absorbed energy. These parameters are obtained from the results of each test configuration and the average values are presented in Table 3.

It can be observed that the variation of the results obtained from the pull-push I test setup is higher than the other two setups and is in the same range as reported in Ghiassi et al. [9]. The specimens tested in the pull-pull configuration have a higher pull-out load (average of 1245 N) when compared to pull-push tests (this value is 987 and 992 N in pull-push I and II tests, respectively). The reason for such an observation can be described by analyzing the global force equilibrium. As shown in Fig. 7a, the applied load (P) in the pull-push tests is equal to the tensile force in the fiber (F), that is balanced by a compressive force in the mortar (M), and the reaction forces in the boundaries (on top of the specimen). On the other hand, in pull-pull specimens tensile forces in the fiber and the mortar balance the applied

load (P), see Fig. 7b. In other words, in the pull-pull test setup, both the fiber bond and the mortar contribute to the tensile resistance, which leads to a higher peak load in these tests. The contribution of the mortar in resisting tensile stresses as well as the gripping conditions in pull-pull configuration can also lead to mortar cracking at the bottom as shown in Fig. 8.

Regarding the initial stiffness, the results from the pull-push I shows the lowest value followed by pull-pull and pull-push II test setups, see Table 3. In this test setup (pull-push I), as explained before, the flexibility of the fibers increases the complexity of the slip measurements. Moreover, due to the space limitations, the LVDTs are usually attached at a small distance from the loaded end and the slip values are measured by reduction of the elastic deformation of the fibers. This adds an additional source of error in the results. Embedment of the fibers in the resin block in pull-push II and pull-pull specimens has therefore a significant role in accurate measurement of the fiber slip during the tests. This resin block eliminates the elastic deformation of the fiber in the un-bonded length and additionally protects the fibers from premature failure due to clamping or stress concentrations during the tests. A comparison between the load-slip curves obtained from the internal LVDT of the hydraulic actuator and the LVDT attached to the fibers in pull-push I and pull-push II test setups clearly confirm the elimination of the elastic deformation of the fibers during the tests (Fig. 9).

The differences in the peak load and initial stiffness of the experimental force-slip curves has also led to a significant difference in the toughness of the specimens. It can be observed in Table 3 that the highest toughness is obtained for the pull-pull tests followed by the pull-push II and pull-push I, as expected.

In addition to the variation of the obtained results, the complexities related to the construction and testing as well as the effectiveness of the test setups is critical. As explained before, preparation of the cylindrical specimens in pull-push I test setup is a difficult task. During the installation of the fibers inside the molds, complete alignment of the fibers is extremely challenging and difficult to control [9]. Additionally, a pre-load shall be applied to specimens in pull-pull I test specimens to ensure a straight alignment of the fiber at the loaded end and to facilitate installation of the LVDT before initiation of the tests. These problems have been resolved in the pull-push II and pull-pull specimens by preparing disk shaped molds for the mortar and embedment of the free length fiber in a block of epoxy resin. Gripping of the pull-pull specimens from the bottom, however, remain tricky as it can lead to crushing/cracking of the mortar before starting of the tests.

4 Pullout mechanism

The fiber pullout problem is usually composed of a reinforcing element, a matrix, and the interfacial region. This interfacial region, depending on the stress level and distribution, can involve the bonded, the debonded, and the sliding zones (Fig. 10. The schematics of test parameters during a pull-out-slip testFig. 10). These zones occur during the pull-out test consecutively or simultaneously throughout the embedded length of the fiber. The pullout curve, as shown in Fig. 11, typically consists of three stages namely: elastic, nonlinear, and dynamic stages [9,25,26,34,38]. In the elastic stage, a perfect bond exists between the fiber and the mortar and the adhesive bond is active. In the nonlinear stage, debonding initiates and the response becomes nonlinear due to the progressive destruction of the adhesive bond. The debonding continues in the post-peak area until the entire bonded length

becomes debonded. At this stage, also called dynamic stage, the only resisting mechanism is friction between the textile and the matrix.

A non-linear relationship is assumed here for the bond stress-slip response of the textile-to-mortar interface [38], see Fig. 11. In the first stage, the stresses are in the elastic range of the bond-slip law until the bond strength τ_{max} is reached. In this stage, the applied load is still less than the maximum bonded load and the fiber and the matrix are fully bonded as shown in Fig. 11a. As the load is increased, debonding initiates at the loaded end and progressively extends towards the free end. Along the debonded length, u, the frictional shear stress, τ_f is active whereas in the rest of the bonded length, L-u, the fiber remains perfectly bonded to the matrix. A shear strength criterion with a constant frictional stress along the debonded zone and a shear-lag model terminating with τ_{max} at the debonding junction characterize the nonlinear stage as shown in Fig. 11b. As a rule, τ_f cannot exceed τ_{max} or be sustained for large slips [38,39]. The dynamic response stage may occur in two conditions: complete debonding (Fig. 11c) and a rigid body motion (Fig. 11d). It is assumed that until the fiber is completely debonded, the shear resistance remains, τ_f [26]. Upon complete debonding, the textile begins a rigid body motion and the resisting shear stress is dropped to dynamic shear strength, τ_{dyn}, [34]. Linear [26] and exponential [38] decay models are proposed in the literature for the dynamic stage. An exponential model is considered here for simulations, although the linear model can also be easily implemented in the same formulations.

5 Mathematical formulation

Analytical modeling of the pull-out response is usually performed following the shear-lag model. In this model, it is assumed that the displacements and the tractions are continuous at the interface and the slip is obtained from the frictional and the adhesive bond. In addition, it is assumed that sliding along a debonded interface is governed by a constant shear stress τ [40–42] while other models utilize a Coulomb's friction law to study this problem [43]. This model has been extensively used for analysis of pull-out problems in cementitious based matrices [26,34,35,38,39,44] and is therefore also used in this study. Here, the formulation proposed by Naaman et al. [38,39] is used for the pull-pull test configuration, see appendix for the details of the formulations. Banholzer et al. [45] reported that if the ratio between the mortar stiffness (A_mE_m) and that of the fiber (A_fE_f) is larger than 10 ($A_mE_m/ A_fE_f >10$), as is the case in this study, the difference the pull-pull and pull-push tests is negligible and the same formulations can be used. Nevertheless, the Namman's formulations are modified here for the pull-push configuration and the observed differences are discussed in Sec. 5.1 to 5.4.

5.1 Basic equations

The mathematical model of the pull-out behavior based on the stress criterion is expressed by two boundary conditions and a second-order differential equation. The equations are derived from the compatibility requirement and the Hooke's law assuming the mortar behaves as an elastic material [26,38,46]. The free-body diagram of the embedded length of the textile in the matrix, as shown in Fig. 10, leads to:

$$F + dF - F - \tau\, dx\, \psi = 0 \Rightarrow \frac{dF}{dx} = \tau\psi = t \quad \text{..... (1)}$$

where F is the local force in the fiber at distance x from the embedded end of the fiber, ψ is the perimeter of the fiber, τ and t are the shear stress and shear flow at the fiber-matrix interface, respectively.

Furthermore, the static equilibrium in the pull-push tests requires that the sum of the local force in the fiber, F, and in the matrix, M, to be equal to zero (Fig. 7a):

$$F + M = 0 \Rightarrow F = -M \quad \text{.....(2)}$$

According to the Hook's law, the local force in the fiber and the matrix can be related to the local strain in the fiber, ε_f, and the mortar, ε_m, as follows:

$$F = A_f E_f \varepsilon_f \Rightarrow \varepsilon_f = \frac{F}{A_f E_f} \quad \text{.....(3)}$$

$$M = A_m E_m \varepsilon_m \Rightarrow \varepsilon_m = \frac{M}{A_m E_m} \quad \text{.....(4)}$$

where A is the cross-sectional area and E is the Young's modulus. The subscripts f and m refer to the fiber and the matrix, respectively. During the elastic stage, the local shear stress, τ, follows a linear stress-slip relationship (Fig. 11a), and is related to the local slip, S, as follows:

$$\tau = \kappa S \quad \text{.....(5)}$$

where κ is the bond shear modulus (slope of the shear strength diagram in the elastic stage in Fig. 11a) and S is defined as:

$$S = \left(\delta_f - \delta_m\right) = \int_0^x \left[\varepsilon_f(x) - \varepsilon_m(x)\right] d_x \quad \text{.....(6)}$$

δ_f and δ_m are the elongation of the fiber and the matrix, respectively. Substituting Eqs. (6, 5) into Eq. (1) and taking the differentiation from x leads to:

$$\frac{d^2F}{dx^2} = \psi\kappa\left(\varepsilon_f - \varepsilon_m\right) \quad \text{.....(7)}$$

By considering Eq. (2) and replacing ε_f and ε_m from Eqs. (3, 4) in Eq. (7), we have:

$$\frac{d^2F}{dx^2} = \psi\kappa FQ \quad \text{.....(8)}$$

where

$$Q = \frac{1}{A_f E_f} + \frac{1}{A_m E_m} \quad \text{.....(9)}$$

Eq. (8) is a second order differential equation and can be rewritten as:A

$$\frac{d^2F}{dx^2} - \lambda^2 F = 0 \quad \text{.....(10)}$$

and

$$\lambda = \sqrt{\kappa\psi Q} \quad \text{.....(11)}$$

The general and particular solution of this nonhomogeneous-second order differential equation is:

$$F_{(x)} = A'e^{\lambda x} + B'e^{-\lambda x} \quad \text{.....(12)}$$

According to the test mechanism, the force boundary condition is equal to zero at the free end, and equal to the applied pull-out load, P, at the loaded end:

$$F_{(0)} = 0 \quad \text{.....(13)}$$

$$F_{(L)} = P \quad \text{.....(14)}$$

Imposing these boundary conditions to Eq. (12), the force distribution along the embedded length and the interfacial shear flow, $t_{(x)}$, are obtained:

$$F_{(x)} = P\frac{\sinh(\lambda x)}{\sinh(\lambda L)} \quad (15)$$

$$t_{(x)} = \frac{dF}{dx} = P\lambda\frac{\cosh(\lambda x)}{\sinh(\lambda L)} \quad (16)$$

The corresponding shear stress can then be derived from Eq. (1) and (16):

$$\tau_{(x)} = \frac{P\lambda}{\psi}\times\frac{\cosh(\lambda x)}{\sinh(\lambda L)} \quad (17)$$

5.2 Elastic stage

If the shear stress at the interface is less than the maximum shear strength, τ_{max}, the applied load will be less than the maximum bonded load and the textile and mortar will be fully bonded. By increasing the load, there will be a critical force, P_{crit}, which causes the shear stress at x=L to be equal to τ_{max}. To find the P_{crit}, the maximum shear stress at x=L is considered:

$$\tau_{max} = \tau_{(x=L)} = \frac{P\lambda}{\psi}\times\frac{\cosh(\lambda L)}{\sinh(\lambda L)} \quad (18)$$

$$P_{crit} = \frac{\tau_{max}\psi}{\lambda}\tanh(\lambda L) \quad (19)$$

The slip at the free end of the fiber can be evaluated by integrating Eq. (6) up to x=L:

$$S = \frac{QP}{\lambda\sinh(\lambda L)}\left(\cosh(\lambda L)-1\right) \quad (20)$$

The slip corresponding to this critical force is obtained by imposing the value of P_{crit} from Eq. (19) in Eq. (20).

5.3 Nonlinear stage

When the applied load, P, exceeds P_{crit}, debonding initiates at the loaded end and grows progressively towards the free end [38]. This means two different interfacial zones coexist along the specimen at this stage. The first one is the debonded zone, in which the interfacial shear stress is equal to the frictional shear strength, τ_f. The forces resisted in this zone are identified as the debonded force, P_d. The remaining zone is still perfectly bonded, as shown in Fig. 11b with the bond force equal to P_b. To satisfy the static equilibrium in the nonlinear stage, for any load larger than P_{crit} and less than the peak load we have:

$$P = P_b + P_d \quad \text{.....(21)}$$

Along the debonded length, u, the normal force distribution in the fiber is linear owing to constant frictional shear strength. This force decreases at the rate of t_f (interfacial frictional shear flow) per unit length:

$$t_f = \tau_f \psi \quad \text{.....(22)}$$

Therefore, P_d can be obtained as:

$$P_d = \tau_f \psi u = t_f u \quad \text{.....(23)}$$

Over the bonded length, L-u, the shear-stress distribution is as explained in the elastic stage, except that the force is P-t_f×u and the length is L-u, as shown in Fig. 11b. For finding the P_b, firstly, the fiber force in the nonlinear stage should be evaluated. In this stage, the force boundary condition is as follows:

$$F_{(x=0)} = 0 \quad \text{.....(24)}$$

$$F_{(x=L-u)} = P - t_f u \quad \text{.....(25)}$$

Imposing these two boundary conditions on Eq. (12), the force distribution and the interfacial shear flow are obtained as:

$$F_{(x)} = \left(P - t_f u\right)\frac{\sinh\left(\lambda x\right)}{\sinh\left(\lambda\left(L-u\right)\right)} \quad \text{.....(26)}$$

$$t_{(x)} = \frac{dF_x}{dx} = \left(P - t_f u\right)\frac{\lambda\cosh\left(\lambda x\right)}{\sinh\left(\lambda\left(L-u\right)\right)} \quad \text{.....(27)}$$

The maximum shear flow and the pull-out force in the nonlinear stage are equal to:

$$t_{(max)} = \frac{\left(P - t_f u\right)\lambda}{\tanh\left(\lambda\left(L-u\right)\right)} \quad \text{.....(28)}$$

$$P = \frac{t_{(max)}}{\lambda}\tanh\left(\lambda\left(L-u\right)\right) + t_f u \quad \text{.....(29)}$$

Eq. (29) includes two parts: bonded and debonded force. Therefore, the bonded force is:

$$P_b = \frac{t_{(max)}}{\lambda}\tanh\left(\lambda\left(L-u\right)\right) \quad \text{.....(30)}$$

The slip can be obtained in the same way as in Eq. (20) considering the bonded and debonded regions as follows:

$$S = Q\left[\int_0^u \left(P - t_f x\right)d_x + \int_0^{L-u} P'\frac{\sinh\left(\lambda x\right)}{\sinh\left(\lambda\left(L-u\right)\right)}d_x\right] \quad \text{.....(31)}$$

$$S = \frac{Qu}{2}\left(2P - t_f u\right) + Q\left(P - t_f u\right)\times\frac{\cosh\left(\lambda\left(L-u\right)\right)-1}{\lambda\sinh\left(\lambda\left(L-u\right)\right)} \quad \text{.....(32)}$$

5.4 Dynamic stage

Two conditions are considered for the dynamic pull-out stage: an initial stage up to complete debonding and a rigid body motion [26,34]. It is assumed that until the fiber is

completely debonded, the shear resistance remains as τ_f. After complete debonding (u= 0), the fiber follows a rigid body motion. For each value of u, a single value exists for the pull-out load and its corresponding end slip. When the dynamic pull-out slip, S_{dyn}, initiates the shear stress drops to the dynamic shear strength, τ_{dyn} and the embedded length decreases to L– v [26,38], in which v is the total rigid body movement of the fiber. The dynamic stage in both pull-push and pull-pull analytical models are equal, because friction is the only the internal force resisting the external force.

As a criteria, the dynamic pull-out slip, S_{dyn}, should be larger than the end slip of the fiber at the onset of full debonding, S_0, and less than the embedded length of the fiber [38]. S_{dyn}, that is equal to the total rigid body movement of the fiber plus the fiber elastic elongation, can be obtained as:

$$S_{dyn} = \frac{Qt_f}{2}(L-v)^2 + v \quad \text{.....(33)}$$

The pull-out force in the dynamic stage depends on the friction between the fiber and the matrix, the Poisson's effect and the effect of decay in Misfit (deteriorates and decreases during the fiber pull-out) [38], and is equal to pull-out [38]:

$$P_{dyn} = \left(1-\exp\left\{\frac{-2\upsilon_f \mu x}{E_f r_f\left[\frac{(1+\upsilon_m)}{E_m}+\frac{(1+\upsilon_f)}{E_f}\right]}\right\}\right)\frac{\delta E_f \pi r_f}{\upsilon_f} \quad \text{.....(34)}$$

where, δ is the coefficient of fiber-matrix misfit and x is the embedded length of the fiber. Also, ν_f and ν_m are the Poisson's ratio for the fiber and the mortar, respectively. r_f is fiber radius and μ is the friction coefficient assumed as 0.06. The formula for obtaining δ can be

found in [38]. S_0 or pull-out end slip at full debonding can be calculated from Eq. (32) in which u= L and P= t_f L [38]:

$$S_0 = \frac{QL^2}{2} t_f \quad \text{.....(35)}$$

To determine an equivalent value for the dynamic shear strength, τ_{dyn}, for any given pull-out load in which slip is more than S_0, the following relation is suggested by Naaman et al. [38]:

$$\tau_{dyn} = \frac{P_{dyn}}{\psi L}, S \geq S_0 \quad \text{.....(36)}$$

6 Pull-out simulation

Analytical modeling of the fiber pull-out response consists of a primary and a secondary problem [39]. In the primary problem, the bond-slip relationship is extracted from the experimental pull-out load-slip curves. Three main parameters namely the peak load, P_p, the corresponding end slip, S_p, and the slope of the initial portion of the curve, P/S (see Fig. 11) have to be extracted from the pull-out curve for solving this problem. These parameters are used to obtain the key parameters of the characteristic bond-slip curves: κ, τ_f, τ_{max}, and S_0. In the secondary problem, the pull-out curve is predicted from the obtained bond-slip law.

6.1 Primary problem

Given an experimental pull-out load-slip curve, the local bond-slip law can be theoretically obtained for a given fiber by calculating the κ, τ_{max}, and τ_f. The bond modulus, κ, is determined as follows:

$$\kappa = \frac{\lambda^2}{\psi Q} \quad \text{.....(37)}$$

where, Q can be obtained from Eq. (9) using the physical and mechanical properties of the fiber, and λ can be solved following an iterative approach from Eq. (20):

$$\left(\frac{P}{S}\right) = \frac{\lambda \sinh(\lambda L)}{Q(\cosh(\lambda L) - 1)} \quad \text{.....(38)}$$

where, P/S is the slope of the linear ascending portion of the experimental pull-out curve. For obtaining the bond strength, τ_{max}, and the frictional bond, τ_f, the peak load, P_p, and its corresponding end slip, S_p, are extracted from the experimental pull-out response curves. As the peak load occurs under partial debonding conditions, its corresponding displacement, u_p, can be calculated from Eq. (29) as:

$$\left(\frac{dP}{du}\right)_{@u=u_p} = 0 \Rightarrow t_f - t_{(max)}\left(1 - \tanh^2\left(\lambda\left(L - u_P\right)\right)\right) = 0 \quad \text{.....(39)}$$

If using P_P, S_P, and u_p instead of P, S, and u, respectively, in Eqs. (29) and (32), the following equations will be obtained:

$$P_P = \frac{t_{(max)}}{\lambda}\tanh\left(\lambda\left(L - u_p\right)\right) + t_f u_p \quad \text{.....(40)}$$

$$S_P = \frac{Qu_P}{2}\left(2P_P - t_f u_P\right) + Q\left(P_P - t_f u_P\right) \times \frac{\cosh\left(\lambda\left(L - u_P\right)\right) - 1}{\lambda \sinh\left(\lambda\left(L - u_P\right)\right)} \quad \text{.....(41)}$$

This leads to a system of three nonlinear equations (39, 40, 41) and three unknowns (t_f, t_{max}, and u_p) that can be solved to obtain the unknown parameters. Once t_f, t_{max}, and u_p are obtained, the τ_f and τ_{max} can be calculated as follow:

$$\tau_f = \frac{t_f}{\psi} \quad \text{.....(42)}$$

$$\tau_{max} = \frac{t_{max}}{\psi} \quad \text{.....(43)}$$

As a controlling criteria, the obtained value of u_p must be between zero and the embedded length. With the four basic parameters κ, τ_{max}, τ_f, and S_0 known, the whole bond-slip relationship can be constructed.

6.2 Secondary problem

The procedure for modeling the pull-out behavior from a given bond-slip relationship can be summarized as follows [38]:

a) In the elastic stage, assume P_i and calculate the slip from Eq. (20). Keep increasing the P_i until it reaches to P_{crit} (Eq. 19).

b) In the nonlinear stage, keep imposing the debonded length u, calculate the corresponding pull-out force (Eq. 29), and end slip (Eq. 32). The value of u is taken between zero and the embedded length of the fiber, L. As a snap back is not observed in a fiber pull-out experiment, this stage is terminated when the slip decreases or become larger than the fully debonded slip (Eq. 35).

c) In the dynamic stage, v is assumed and S_{dyn} is calculated from Eq. (33). For each value of the end slip S_{dyn} ($S_0 \leq S_{dyn} \leq L$), the load can be obtained from Eq. (34), where $x = L - S_{dyn} - S_0$. v is increased and the calculation is repeated to obtain a full range response.

6.3 Comparison with experimental results

A comparison is made here between the obtained experimental results and analytical simulations for all the considered test setups. The input parameters for these simulations are mechanical and geometrical properties of the fiber and the mortar as well as the

experimental force-slip curves. The modulus of elasticity of the fiber and the mortar are equal to 174.87 GPa (obtained from experimental tests) and 9.23 GPa (given in the technical datasheets), respectively. The Poisson's ratio of the fiber and the mortar are taken as 0.3 and 0.2, respectively. The parameters P_P, S_P, and P/S are obtained from the experimental load-slip curves as explained in Sec. 5.1. The effective area of the mortar, A_m, is usually assumed as 100 times of the fiber ($A_m=\alpha A_f$, $\alpha=100$) [39]. However, a survey of the literature indicated that the effective load carrying area of the matrix has not been determined explicitly [46]. The effect of this parameter on the analytical results is therefore discussed in the next section. Having the above mentioned properties, the key parameters of the bond-slip curve (λ, κ, τ_{max}, τ_f, S_0) are calculated by solving Eqs. (37-43). With the aim of the obtained bond-slip curves, the secondary problem is then solved to predict the pull-out force-slip curves.

Fig. 12 shows the analytical load-slip curves and bond-slip laws obtained for all the test setups considering different values for the effective mortar area (by changing the α value). It can be instantly seen that this parameter has a significant effect on the obtained results. As explained before, obtaining an accurate answer for the differential equations presented in sec. 5 requires satisfaction of all three Eqs. (39-41), as well as having the obtained u_p and S_{max} less than the embedded length and the S_0, respectively.

Here, in the pull-push I tests, although almost all α values (from 50 to 3700) produce acceptable pull-out curves with respect to the experimental envelop, Fig. 12a, and show small changes in the bond-slip laws, Fig. 12b, the convergence criteria are fellfield only for α values larger than 500. On the other hand, all the considered α values fulfill the convergence criteria in pull-push II and pull-pull configurations, Fig. 12c-f, but only α

values of 55 and 100 produce acceptable results (similar to the value proposed in [39]) in comparison to experimental envelope (best results are for α=55 in pull-push II and α=100 in pull-pull configurations).

The effect of α on the bond-slip laws seems significant in pull-push II and pull-pull configurations. This is clearer in Fig. 13 where the changes of bond-slip law parameters with α are presented. It can be observed that by increasing α (and correspondingly A_m), the τ_{max} increases while the τ_f decreases in both test configurations until $500<\alpha<1900$ where these values does not change anymore with the change of α. The effect of α on the bond modulus is contrary in pull-push II and pull-pull tests, i.e. its increase leads to increment of bond modulus in pull-push II and its decrement in pull-pull configuration. It should also be noted that the τ_{max} and τ_f are in the same range in both pull-push II and pull-pull tests for $\alpha<500$, after which these values converge significantly.

Banholzer et al. [45] reported that if the ratio between the mortar stiffness (A_mE_m) and that of the fiber (A_fE_f) is larger than 10 ($A_mE_m/ A_fE_f >10$), the difference the pull-pull and pull-push tests is negligible and the same formulations can be used. In this study, if the mortar area is equal to 200 times of the fiber (assuming $\alpha =200$), the stiffness ratio of mortar and fiber becomes larger than 10. Comparison between the analytical results of both pull-push and pull-pull configurations, however, shows that the bond properties and their corresponding load-slip curves are not similar to each other, see Fig. 12 and Fig. 13. Although, it should be noted that the input values (the ones that are taken from the experimental force-slip curves) for the simulations are also different in these cases and this may be the reason for the observed differences in the pull-pull and pull-push configurations.

For this reason, a new analysis is performed considering the same input values but different α, and the bond-slip laws and pull-out curves are produced for both pull-push and pull-pull configurations, see Fig. 14. It can be observed that even when the input values are similar, in both case of α=55 (corresponding to an A_mE_m/ A_fE_f=2.90) and α=200 (corresponding to an A_mE_m/ A_fE_f=10.56) the results obtained from pull-pull and pull-push configurations are different. On the other hand, if the simulations are performed on experimental results produced by Naaman et al. [39] (specimen H2SL with mortar compressive strength and elastic modulus of 60.2 MPa and 21 GPa, respectively), Fig. 15, it can be seen that the results from pull-pull and pull-push simulations are similar when an α=100 (corresponding to an A_mE_m/ A_fE_f=10) is used while they are different when this values is changed to 50 (corresponding to an A_mE_m/ A_fE_f=50). These results show that the A_mE_m/ A_fE_f ratio is not a sufficient criterion for evaluating the applicability of pull-pull formulations in pull-push test configuration. Indeed, it seems that the ratio of A_m/A_f and E_m/E_f have to be evaluated separately with different criteria.

Having considered the above-mentioned issues, the effect of test setup on the extracted bond-slip laws is summarized in Table 4 and Fig. 16. A comparison between the experimental and analytical results of pull-push I and II illustrates that increment of the initial stiffness of the pull-out curves (as is the main difference between these two tests), leads to increment of the bond modulus in pull-push II tests. Meanwhile, the τ_{max} and τ_f are approximately equal in both pull-push I and II tests. On the other hand, in pull-pull configuration, the bond modulus is lower than, the τ_f is higher than and the τ_{max} is similar to pull-push configuration results.

For further verification of the observed response and drawn conclusions on the pull-out behavior in different test setups, finite element (FE) simulations are performed next. For simulations, 8-node solid elements and 2-node truss elements (with a 5 mm mesh size) are utilized to model the mortar and the fiber, respectively. Interface elements are also used to simulate the bond behavior between the mortar and the fiber, in which the bond-slip-laws obtained from the analytical modeling is employed, see Fig. 17. The independency of the results to the mesh size is also investigated. The distributions of stresses in the mortar at the peak load in pull-pull and pull-push configurations are presented in Fig. 18. It can be observed that most of the mortar in the pull-push configuration is under compressive stresses, caused due to the tensile load in the fiber, and only a small region near the loaded end is under tensile stresses, Fig. 18a. On the other hand, the mortar is completely under tensile stresses in the pull-pull configuration (Fig. 18b). These observations confirm the assumptions made for development of the analytical formulations. A comparison between the numerical and analytical results is presented in Fig. 19 and Table 5 for all the considered test setups. The outcomes, besides a slight difference between numerical and analytical results, illustrate a good agreement between these modeling strategies. In addition, the pull-out properties of numerical modeling are shown in Table 5. It should be noted that the abrupt changes after the peak load are owing to the sudden change of the nonlinear stage to the dynamic stage. This observation has also been reported by other researchers [26,34,39].

7 Conclusions

A comprehensive experimental, analytical and numerical study is presented in this paper for evaluating the effect of test setup and specimens configurations on the fiber-to-mortar bond response in TRM composites. To this aim, a series of pull-out tests are performed on steel fibers embedded in a hydraulic lime based mortar utilizing three conventional test setups including two pull-push and one pull-pull configurations.

The results show that the pull-push test setup when the free length of the fiber is embedded in an epoxy resin (pull-push II setup) is the most reliable test setup and produced the lowest variation of the results (CoVs). The embedment of the fibers in the free length with a resin block prevents premature failure of the fibers. It also facilitates attachment of the LVDTs for slip measurements during the tests. The advantage of using the block resin becomes even clearer when fibers with low axial stiffness or with a woven structure are under investigation. Installation of the specimens on the test setup when the fibers are not embedded in the epoxy resin (case of pull-push I in the current study) is also found very challenging and time-consuming. Application of a pre-loading is also necessary in these specimens before performing the tests to facilitate the LVDTs attachment.

As for preparation of the specimens, ensuring the straight alignment of the fibers in the mortar is also very complicated when cylindrical mortars (case of pull-push I in the current study) are used. This is resolved by designing disk shaped molds that allowed application of the mortar in two layers parallel to the fiber embedment direction, and the perfect alignment of the fibers (case of pull-push II and pull-pull configurations).

The contribution of the mortar in resisting tensile forces in the pull-pull configuration leads to larger experimental peak load and toughness in comparison to the pull-push configuration. It is also observed that gripping of the mortar from the bottom in this configuration could lead to mortar cracking/crushing before performing the tests.

With the aim of analytical and numerical modeling, the bond-slip laws are extracted from the experimental results obtained corresponding to each test setup. The results show that the differences in the load-slip curves of the specimens tested in different test setups can lead to different bond-slip laws.

8 Acknowledgements

This work was partly financed by FEDER funds through the Competitivity Factors Operational Programme (COMPETE) and by national funds through the Foundation for Science and Technology (FCT) within the scope of project POCI-01-0145-FEDER-007633. The support to the first author through grant SFRH/BD/131282/2017 is acknowledged. The second author acknowledges the financial support of the European Union's Marie Curie Individual Fellowship program under REA grant agreement No. 701531.

9 Symbols

A_f	The cross-sectional area of fiber
A_m	The cross-sectional area of mortar
E_f	Young's modulus of fiber
E_m	Young's modulus of mortar
ε_f	The local strain in the fiber
ε_m	The local strain in the mortar
F	The local force in the fiber
L	The embedded length of fiber in a mortar
M	The local force in the mortar
P	The total force
P/S	The slope of the initial portion of experimental pull-out curve
P_b	Bonded force
P_{crit}	Critical pull-out load
P_d	Debonding force
P_p	The peak load obtained from experimental pull-out curves
r_f	Fiber radius
S	The local slip between fiber and mortar
S_0	Relative slip of the fiber at full debonding
S_p	Slip corresponding to the peak load obtained from experimental pull-out curve
t_f	Interfacial frictional shear flow
t_{max}	Maximum allowable interfacial shear flow
u	Debonding length
δ	The coefficient of fiber-matrix misfit
δ_f	The elongation of the fiber
δ_m	The elongation of the mortar
κ	The bond modulus
μ	Friction coefficient, assumed 0.2
ν_f	Poisson ratio of fiber
ν_m	Poisson ratio of mortar
τ	The shear at the fiber-matrix interface
τ_{dyn}	The dynamic shear strength
τ_f	Maximum frictional bond shear stress
τ_{max}	The maximum shear strength
ψ	The perimeter of the fiber

10 References

[1] Carozzi FG, Poggi C. Mechanical properties and debonding strength of Fabric Reinforced Cementitious Matrix (FRCM) systems for masonry strengthening. Compos Part B Eng 2015;70:215–30. doi:10.1016/j.compositesb.2014.10.056.

[2] de Felice G, De Santis S, Garmendia L, Larrinaga P, Lourenço PB, Oliveira D V, et al. Mortar-based systems for externally bonded strengthening of masonry. Mater Struct 2014;47:2021–37. doi:10.1617/s11527-014-0360-1.

[3] Razavizadeh A, Ghiassi B, Oliveira D V. Bond behavior of SRG-strengthened masonry units: Testing and numerical modeling. Constr Build Mater 2014;64:387–97. doi:10.1016/j.conbuildmat.2014.04.070.

[4] Papanicolaou CG, Triantafillou TC, Papathanasiou M, Karlos K. Textile-reinforced mortar (TRM) versus FRP as strengthening material of URM walls : in-plane cyclic loading. Mater Struct 2007;40:1081–97. doi:10.1617/s11527-006-9207-8.

[5] De Santis S, de Felice G. Steel reinforced grout systems for the strengthening of masonry structures. Compos Struct J 2015;134:533–48. doi:10.1016/j.compstruct.2015.08.094.

[6] Barr S, Mccarter WJ, Suryanto B. Bond-strength performance of hydraulic lime and natural cement mortared sandstone masonry. Constr Build Mater 2015;84:128–35. doi:10.1016/j.conbuildmat.2015.03.016.

[7] Pavlík V, Uzáková M. Effect of curing conditions on the properties of lime, lime – metakaolin and lime – zeolite mortars. Constr Build Mater 2016;102:14–25. doi:10.1016/j.conbuildmat.2015.10.128.

[8] Lanas J, Pe JL, Bello MA, Alvarez JI. Mechanical properties of masonry repair dolomitic lime-based mortars. Cem Concr Res 2006;36:951–60. doi:10.1016/j.cemconres.2005.10.004.

[9] Ghiassi B, Oliveira D V, Marques V, Soares E, Maljaee H. Multi-level characterization of steel reinforced mortars for strengthening of masonry structures. Mater Des 2016;110:903–13. doi:10.1016/j.matdes.2016.08.034.

[10] Larrinaga P, Chastre C, San-José JT, Garmendia L. Non-linear analytical model of composites based on basalt textile reinforced mortar under uniaxial tension. Compos Part B Eng 2013;55:518–27. doi:10.1016/j.compositesb.2013.06.043.

[11] Caggegi C, Carozzi FG, De Santis S, Fabbrocino F, Focacci F, Hojdys Ł, et al. Experimental analysis on tensile and bond properties of PBO and aramid fabric reinforced cementitious matrix for strengthening masonry structures. Compos Part B Eng 2017;127. doi:10.1016/j.compositesb.2017.05.048.

[12] Leone M, Aiello MA, Balsamo A, Carozzi FG, Ceroni F, Corradi M, et al. Glass fabric reinforced cementitious matrix: Tensile properties and bond performance on masonry substrate. Compos Part B Eng 2017;127. doi:10.1016/j.compositesb.2017.06.028.

[13] Ascione L, De Felice G, De Santis S. A qualification method for externally bonded Fiber Reinforced Cementitious Matrix (FRCM) strengthening systems. Compos Part B Eng 2015;78:497–506. doi:10.1016/j.compositesb.2015.03.079.

[14] Brameshuber W. Textile Reinforced Concrete - State-of-the-Art Report of RILEM TC 201-TRC. 2006.

[15] Robins P, Austin S, Jones P. Pull-out behaviour of hooked steel fibers. Mater Struct 2002;35:434–42. doi:10.1007/BF02483148.

[16] Isla F, Ruano G, Luccioni B. Analysis of steel fibers pull-out. Experimental study. Constr Build Mater 2015;100:183–93. doi:10.1016/j.conbuildmat.2015.09.034.

[17] Banholzer B, Brockmann T, Brameshuber W. Material and bonding characteristics for dimensioning and modelling of textile reinforced concrete (TRC) elements. Mater Struct 2006;39:749–63. doi:10.1617/s11527-006-9140-x.

[18] Yoo DY, Park JJ, Kim SW. Fiber pullout behavior of HPFRCC: Effects of matrix strength and fiber type. Compos Struct 2017;174:263–76. doi:10.1016/j.compstruct.2017.04.064.

[19] Williams Portal N, Fernandez Perez I, Nyholm Thrane L, Lundgren K. Pull-out of textile reinforcement in concrete. Constr Build Mater 2014;71:63–71. doi:10.1016/j.conbuildmat.2014.08.014.

[20] Tuyan M, Yazıcı H. Pull-out behavior of single steel fiber from SIFCON matrix. Constr Build Mater 2012;35:571–7. doi:10.1016/j.conbuildmat.2012.04.110.
[21] Guerrero P, Naaman AE, Energy P. Effect of mortar fineness and adhesive agents on pullout response of steel fibers. ACI Struct J 2000;97:12–20.
[22] Abrishambaf A, Barros JAO, Cunha VMCF, Frazão C. Time dependent behaviour of fiber pull-out in self-compacting concrete. Cem Concr Compos 2017;77:14–28. doi:10.1016/j.cemconcomp.2016.12.004.
[23] Won JP, Lee JH, Lee SJ. Predicting pull-out behaviour based on the bond mechanism of arch-type steel fiber in cementitious composite. Compos Struct 2015;134:633–44. doi:10.1016/j.compstruct.2015.08.127.
[24] Baena M, Torres L, Turon A, Llorens M, Barris C. Bond behaviour between recycled aggregate concrete and glass fiber reinforced polymer bars. Constr Build Mater 2016;106:449–60. doi:10.1016/j.conbuildmat.2015.12.145.
[25] Shannag J, Brincker R, Hansen W. Pullout behavior of steel fibers from cement-based composites. Cem Concr Res 1997;27:925–36. doi:10.1016/S0008-8846(97)00061-6.
[26] Sueki S, Soranakom C, Mobasher B, Asce M, Peled A. Pullout-slip response of fabrics embedded in a cement paste matrix. J Mater Civ Eng 2007;19:718–28. doi:10.1061/(ASCE)0899-1561(2007)19:9(718).
[27] Huang L, Chi Y, Xu L, Chen P, Zhang A. Local bond performance of rebar embedded in steel-polypropylene hybrid fiber reinforced concrete under monotonic and cyclic loading. Constr Build Mater 2016;103:77–92. doi:10.1016/j.conbuildmat.2015.11.040.
[28] Li Y, Bielak J, Hegger J, Chudoba R. An incremental inverse analysis procedure for identification of bond-slip laws in composites applied to textile reinforced concrete. Compos Part B Eng 2018;137:111–22. doi:10.1016/j.compositesb.2017.11.014.
[29] ASTM C109/C109M. Standard Standard test method for compressive strength of hydraulic cement mortars 2005;4.
[30] BS EN 1015-11. Methods of test for mortar for masonry. Determination of flexural and compressive strength of hardened mortar. 1999.
[31] Banholzer B. Bond of a strand in a cementitious matrix. Mater Struct 2006;39:1015–28. doi:10.1617/s11527-006-9115-y.
[32] Committee RT. RILEM TECHNICAL COMMITTEE RILEM TC 203-RHM : Repair mortars for historic masonry 2012:1287–94. doi:10.1617/s11527-012-9847-9.
[33] ASTM C141- Standard specification for hydrated hydraulic lime for structural purposes. 2014. doi:10.1520/C0141_C0141M-14.
[34] Mobasher B. Mechanics of Fiber and Textile Reinforced Cement Composites. London- New York: Taylor & Francis Group; 2012.
[35] Alwan JM, Naaman A, Hansen W. Pull-Out work of steel fibers from cementitious composites : analytical investigation. Cem Concr Compos 1991;13:247–55. doi:10.1016/0958-9465(91)90030-L.
[36] Leung CKY, Geng Y. Effect of lateral stresses on fiber debonding/ pull-out. Compos Eng 1995;5. doi:10.1016/0961-9526(95)00064-T.
[37] Shannag J, Hansen W, Tjiptobroto P. Interface debonding in fiber reinforced cement-matrix composites. J Compos Mater 1999;33:158–76. doi:10.1177/002199839903300203.
[38] Naaman AE, Namur GG, Alwan JM, Najm HS. Fiber pullout and bond slip. i: analytical study. J Struct Eng 1991;117:2769–90. doi:10.1061/(ASCE)0733-9445(1991)117:9(2769).
[39] Naaman AE, Namur GG, Alwan JM, Najm HS. Fiber pullout and bond slip. ii: experimental validation. J Struct Eng 1991;117:2791–800. doi:10.1061/(ASCE)0733-9445(1991)117:9(2791).
[40] Marshall DB. Measurement of Interfacial Mechanical Properties in Fiber-Reinforced Ceramic Composites. J Am Ceram Soc 1987;70:542–8. doi:10.1111/j.1151-2916.1987.tb05702.x.
[41] Hsueh C. Interfacial debonding and fiber pull-out stresses of fiber-reinforced composites. Mater Sci Eng A 1992;154:125–32. doi:10.1016/0921-5093(92)90337-Z.
[42] Marshall DB. Analysis of fiber debonding and sliding experiments in brittle matrix composites. Acta Metall Mater 1992;40:427–41. doi:10.1016/0956-7151(92)90391-Q.
[43] Hutchinson JW. Models of fiber debonding and pullout in brittle composites with friction. Mech Mater 1990;9:139–63. doi:10.1016/0167-6636(90)90037-G.

[44] Gray RJ. Analysis of the effect of embedded fiber length on fiber debonding and pull-out from an elastic matrix Part 2 Application to a steel fiber-cementitious matrix composite system. J Mater Sci 1984;19:1680–91. doi:10.1007/BF00563066.
[45] Banholzer B, Brameshuber W, Jung W. Analytical evaluation of pull-out tests-The inverse problem. Cem Concr Compos 2006;28:564–71. doi:10.1016/j.cemconcomp.2006.02.015.
[46] Banholzer B. Analytical simulation of pull-out tests- the direct problem. Cem Concr Compos 2005;27:93–101. doi:10.1016/j.cemconcomp.2004.01.006.

11 Appendix

The pull-out load versus fiber the end displacement relationship of pull-pull specimens can be summarized in the following equations. These equations are rewritten based on Naaman et al. [38,39].

The critical force and fiber slip in the elastic stage are:

$$P_{crit} = \frac{\tau_{max}\psi}{\lambda} \times \frac{QA_mE_m \sinh(\lambda L)}{\left[\cosh(\lambda L)(QA_mE_m - 1) + 1\right]} \quad \text{(A1)}$$

$$S = \frac{P(\cosh(\lambda L) - 1)}{\lambda \sinh(\lambda L)}\left(Q - \frac{2}{A_mE_m}\right) \quad \text{(A2)}$$

In addition, in the nonlinear stage, the pull-out load, the fiber slip and the pull-out end slip at full debonding are equals to:

$$P = \frac{t_{(max)}}{\lambda} \frac{QA_mE_m \sinh(\lambda(L-u))}{\left[\cosh(\lambda(L-u))(QA_mE_m - 1) + 1\right]} + t_f u \quad \text{(A3)}$$

$$S = \frac{-PL}{A_mE_m} + \frac{Qu}{2}(2P - t_f u) + \frac{P - t_f u}{\lambda A_mE_m} \times \left[\frac{\cosh(\lambda(L-u)) - 1}{\sinh(\lambda(L-u))}(QA_mE_m - 2) + \lambda(L-u)\right] \quad \text{(A4)}$$

$$S_0 = t_f L^2\left(\frac{Q}{2} - \frac{1}{A_mE_m}\right) \quad \text{(A5)}$$

The pull-out load of dynamic stage is calculated from Eq. (34) and its slip is equal to:

$$S_{dyn} = \frac{-P(L-v)}{A_mE_m} + \frac{Qt_f}{2}(L-v)^2 + v \quad \text{(A6)}$$

In order to calculating t_{max} and t_f, the following three equations should solve:

$$t_f - t_{(max)} QA_m E_m \left[\frac{QA_m E_m \sinh\left(\lambda\left(L-u_p\right)\right)}{\left(\cosh\left(\lambda\left(L-u_p\right)\right)\left(QA_m E_m - 1\right)+1\right)^2} \right] = 0 \quad \text{..... (A7)}$$

$$t_f u_p - \frac{t_{(max)}}{\lambda} QA_m E_m \left[\frac{QA_m E_m \sinh\left(\lambda\left(L-u_p\right)\right)}{\left(\cosh\left(\lambda\left(L-u_p\right)\right)\left(QA_m E_m - 1\right)+1\right)} \right] - P_p = 0 \quad \text{..... (A8)}$$

$$\begin{aligned} &\frac{-PL}{A_m E_m} + \frac{Qu_p}{2}\left(2P_p - t_f u_p\right) \\ &+ \frac{-P_p - t_f u_p}{\lambda A_m E_m}\left[\frac{\cosh\left(\lambda\left(L-u_p\right)\right)-1}{\sinh\left(\lambda\left(L-u_p\right)\right)}\left(QA_m E_m - 2\right) + \lambda\left(L-u_p\right) \right] - S_p = 0 \end{aligned} \quad \text{..... (A9)}$$

λ can be calculated from the following equation:

$$\left(\frac{P}{S}\right) = \frac{\lambda \sinh\left(\lambda L\right)}{\left(Q - \frac{2}{A_m E_m}\right)\left(\cosh\left(\lambda L\right)-1\right)} \quad \text{..... (A10)}$$

Q and κ in above equations are obtained from Eqs. (9) and (37), respectively.

List of Figures

(a) (b) (c)

Fig. 1. Mechanical characterization tests: (a) mortar compressive test; (b) mortar flexural test; (c) fiber direct tensile test.

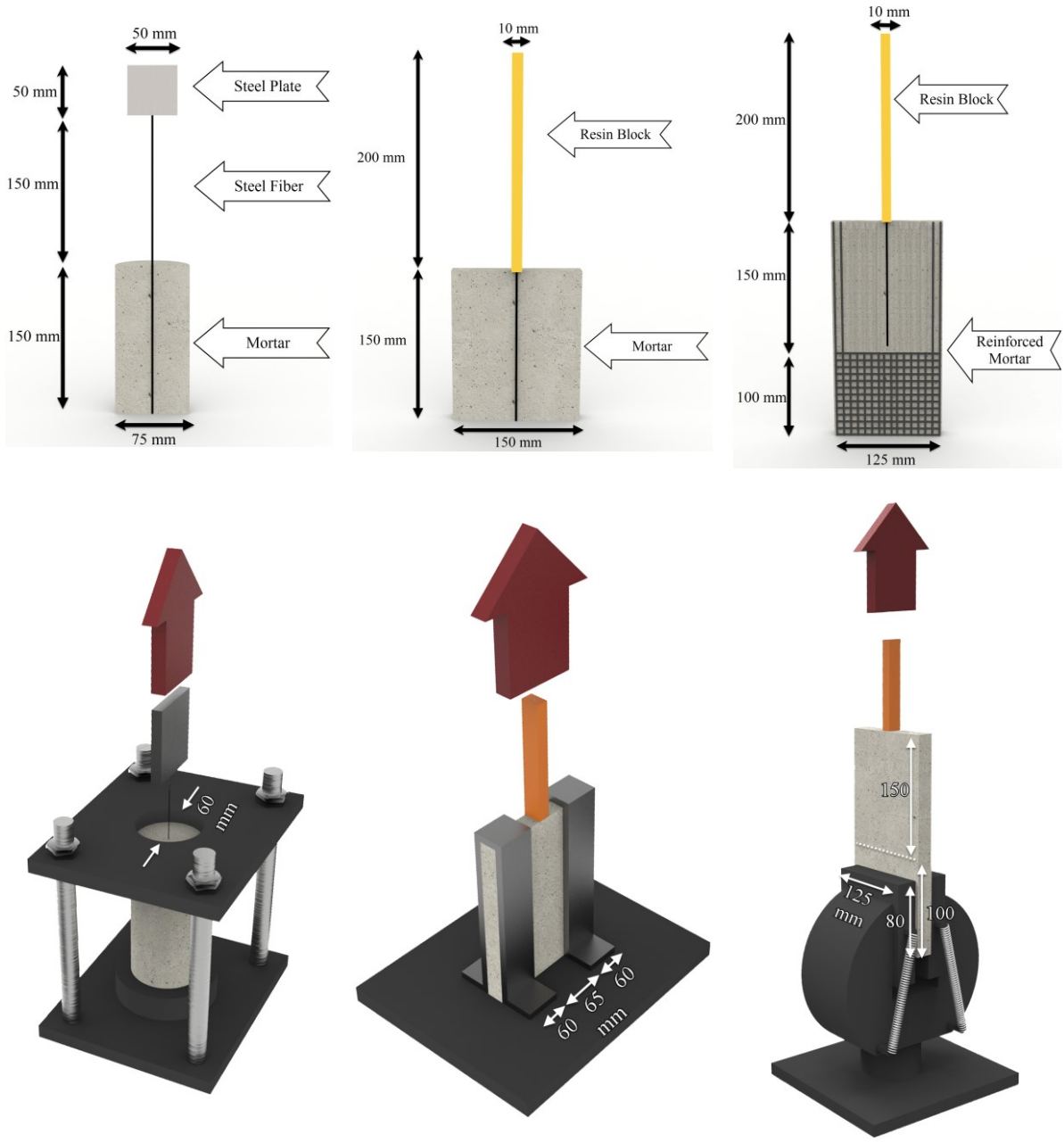

Fig. 2. Specimens' configurations and corresponding test setups: (a) pull-push I; (b) pull-push II; (c) pull-pull.

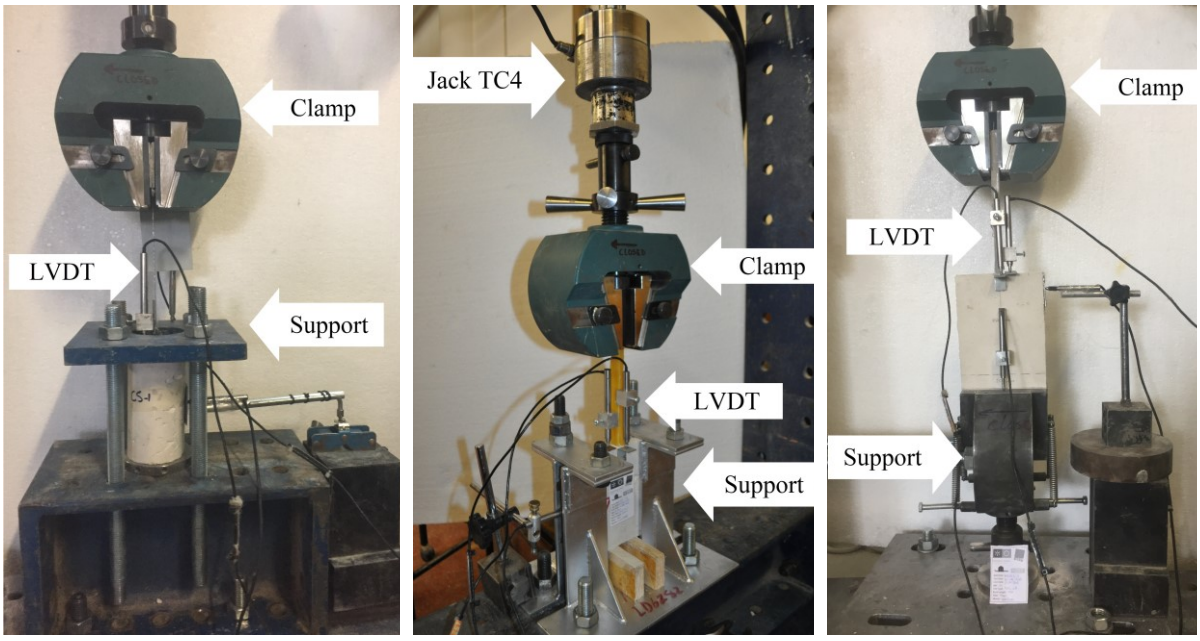

(a) (b) (c)

Fig. 3. Test setups and instrumentation used for pull-out tests: (a) pull-push I; (b) pull-push II; (c) pull-pull.

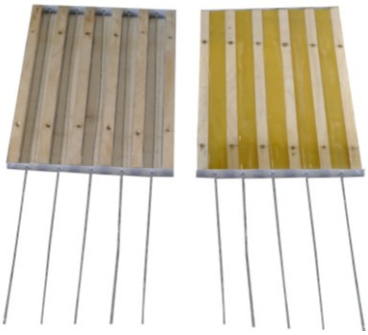

(a)

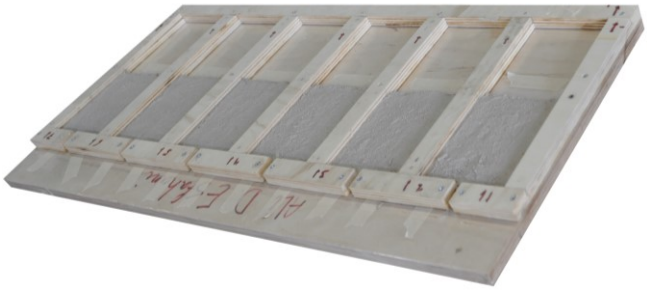

(b)

(c)

Fig. 4. The stages of preparation of the pull-push II specimens: (a) embedment of the fibers in resin; (b) applying first layer of the mortar; (c) adjusting fiber and pouring the second layer of the mortar.

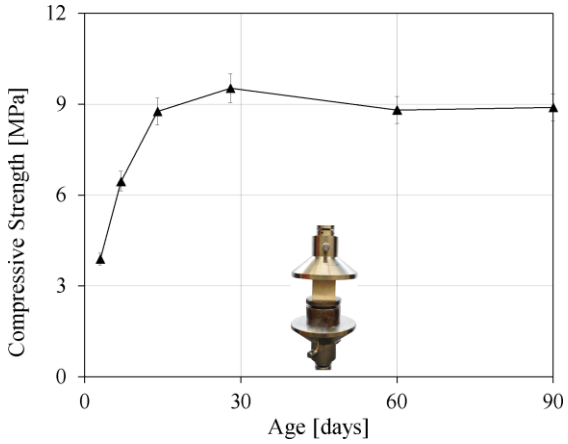

(a)

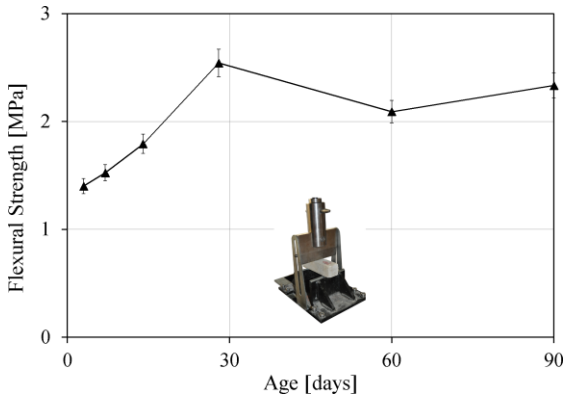

(b)

Fig. 5. Time evolution of mortar strength: (a) compressive strength; (b) flexural strength.

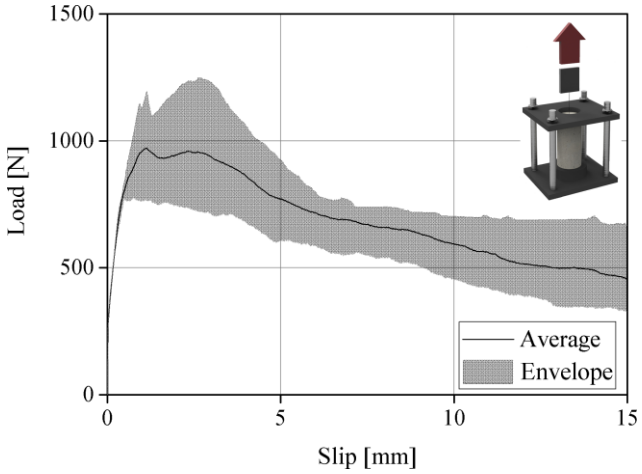

(a)

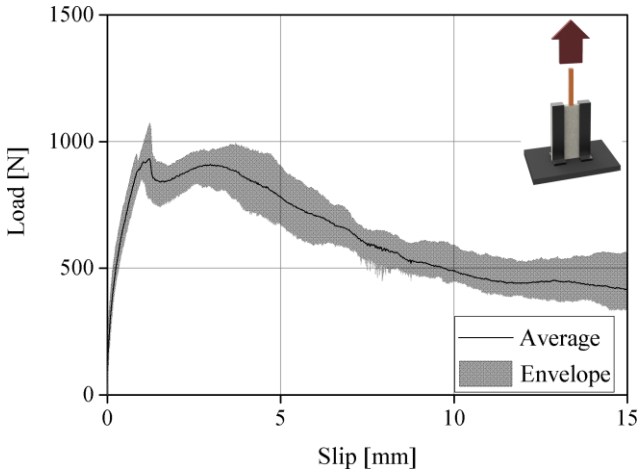

(b)

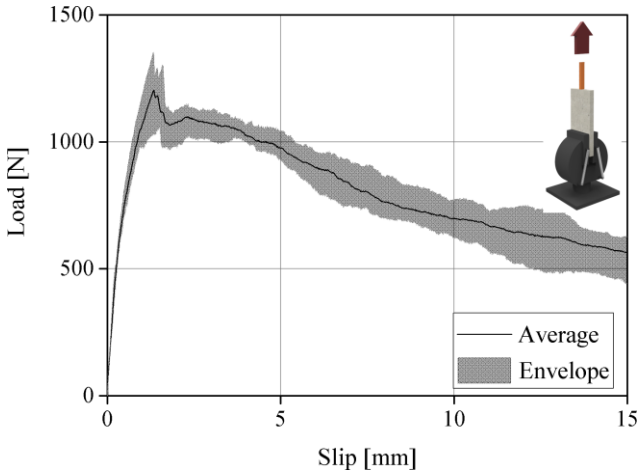

(c)

Fig. 6. Envelope load-slip curves for different test setups: (a) pull-push I; (b) pull-push II; (c) pull-pull.

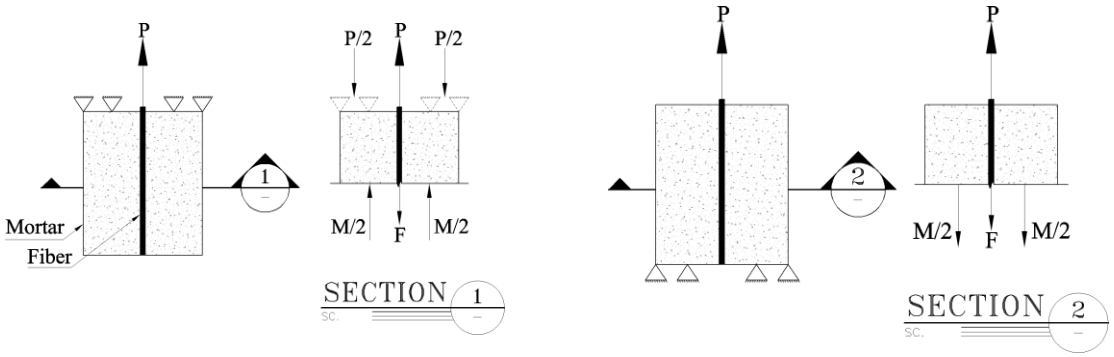

(a) (b)

Fig. 7. Global force equilibrium: (a) pull-push test; (b) pull-pull test.

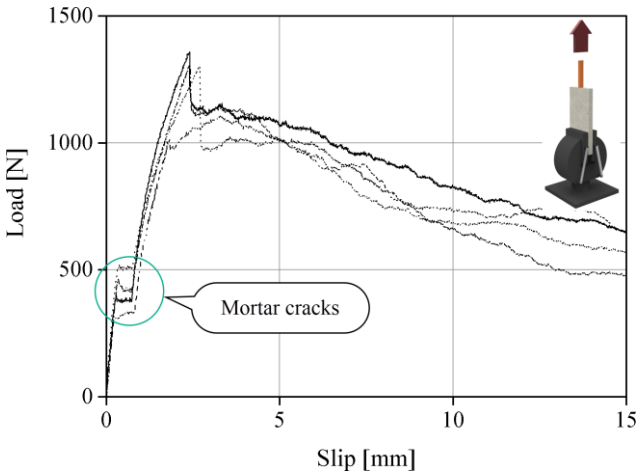

Fig. 8. Load-slip curves of pull-pull specimens obtained from the internal LVDT of the machine.

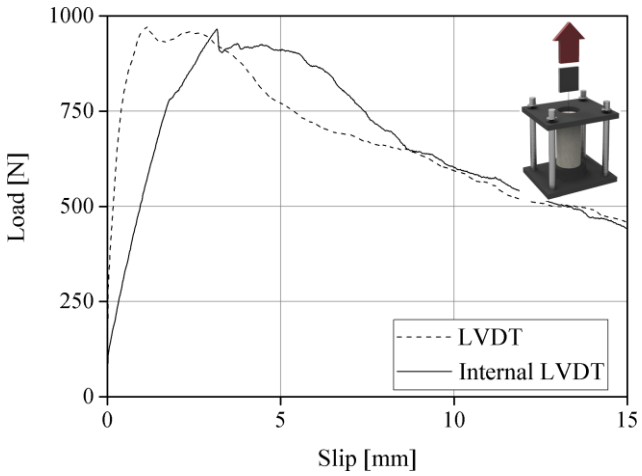

(a)

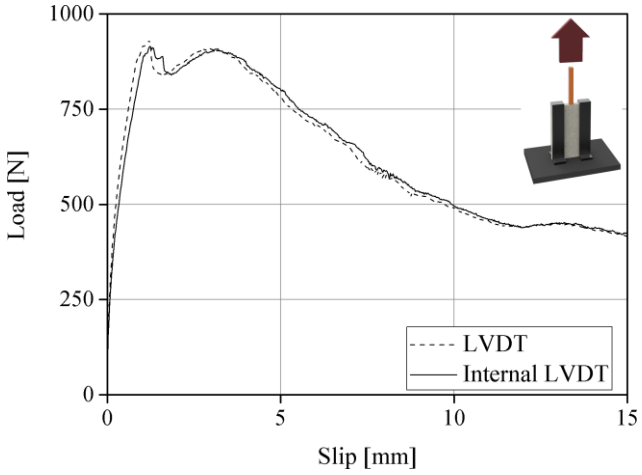

(b)

Fig. 9. Average load-slip curves obtained from LVDT and internal LVDT of the machine: (a) pull-push I; (b) pull-push II.

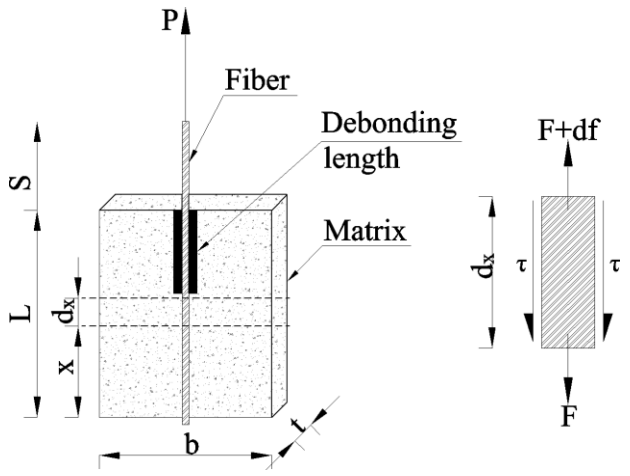

Fig. 10. The schematics of test parameters during a pull-out-slip test.

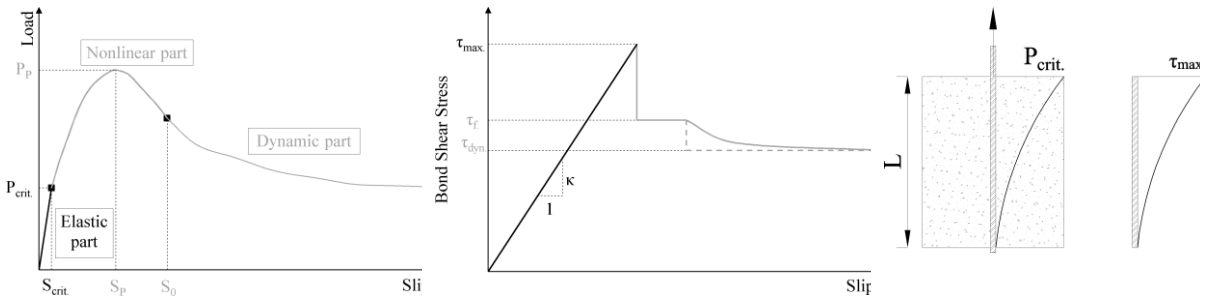

(a)

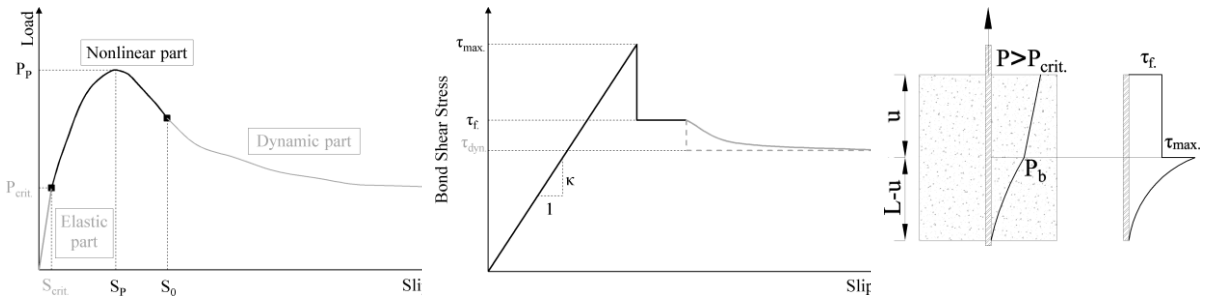

(b)

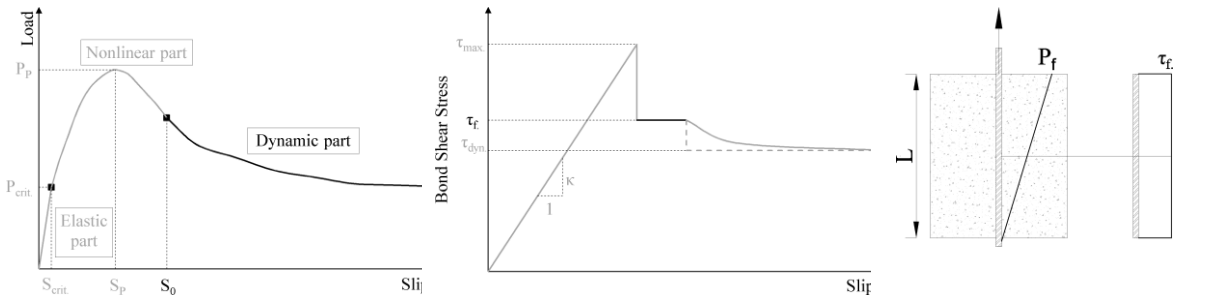

(c)

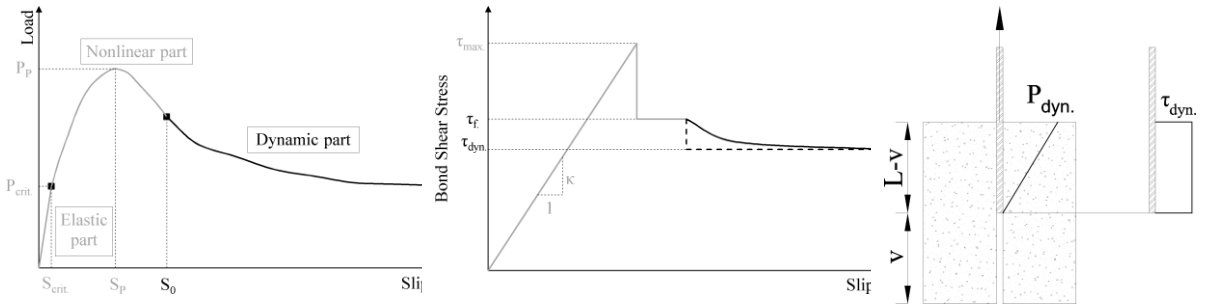

(d)

Fig. 11. Typical pull-out diagram, assumed bond shear stress-slip, and force distribution along the fiber at different stages: (a) linear-elastic; (b) debonding; (c) frictional pull-out; (d) sliding mode.

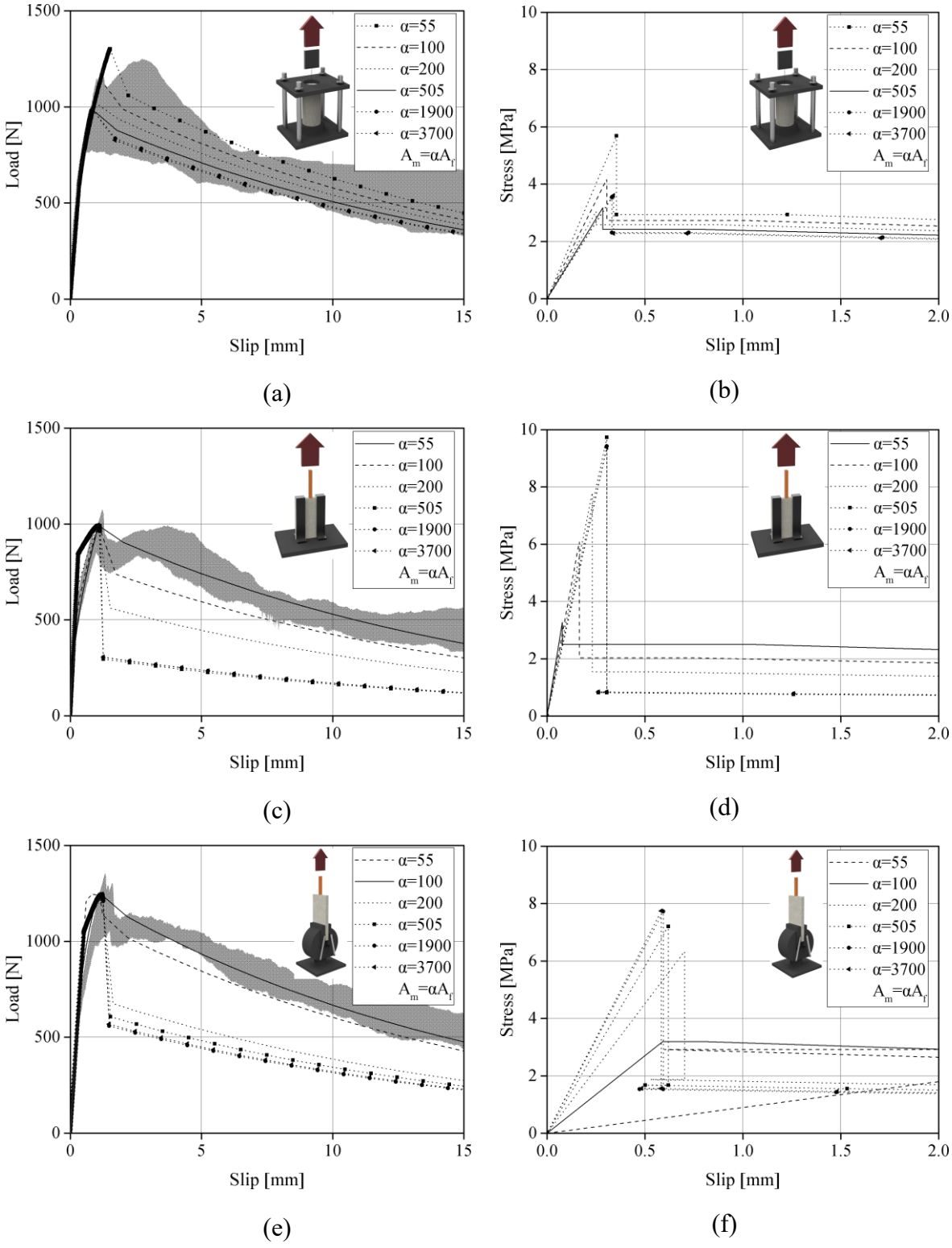

Fig. 12. The results of analytical modeling based on changing mortar area, A_m: (a) and (b) pull-push I; (c) and (d) pull-push II; (e) and (f) pull-pull.

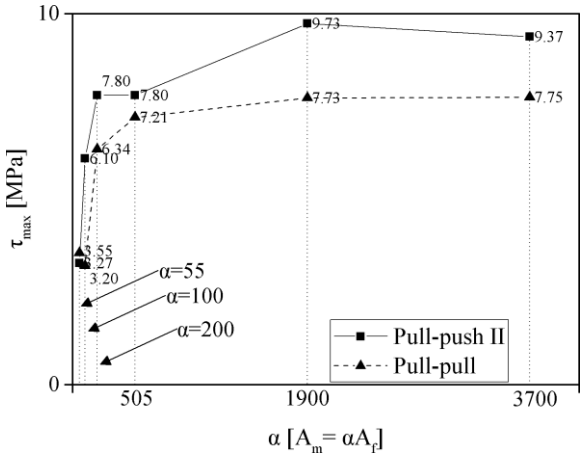

(a)

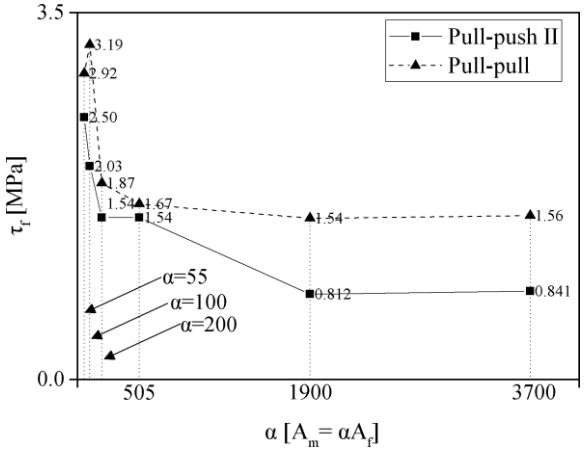

(b)

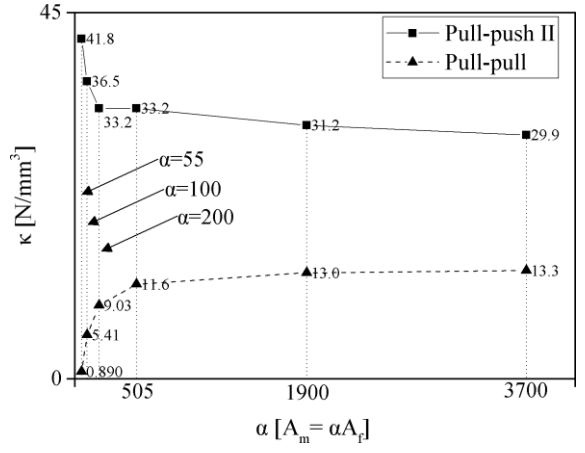

(c)

Fig. 13. Effect of mortar area (A_m) on the bond properties: (a) maximum stress; (b) friction stress; (c) bond modulus.

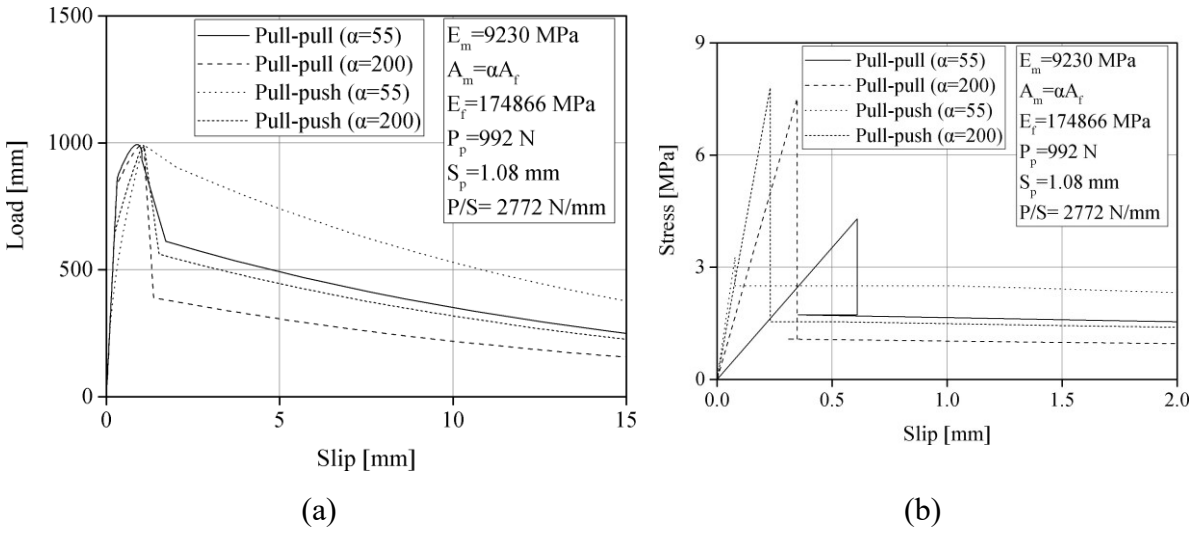

Fig. 14. The effect of pull-pull and pull-push configuration when similar input values are used.

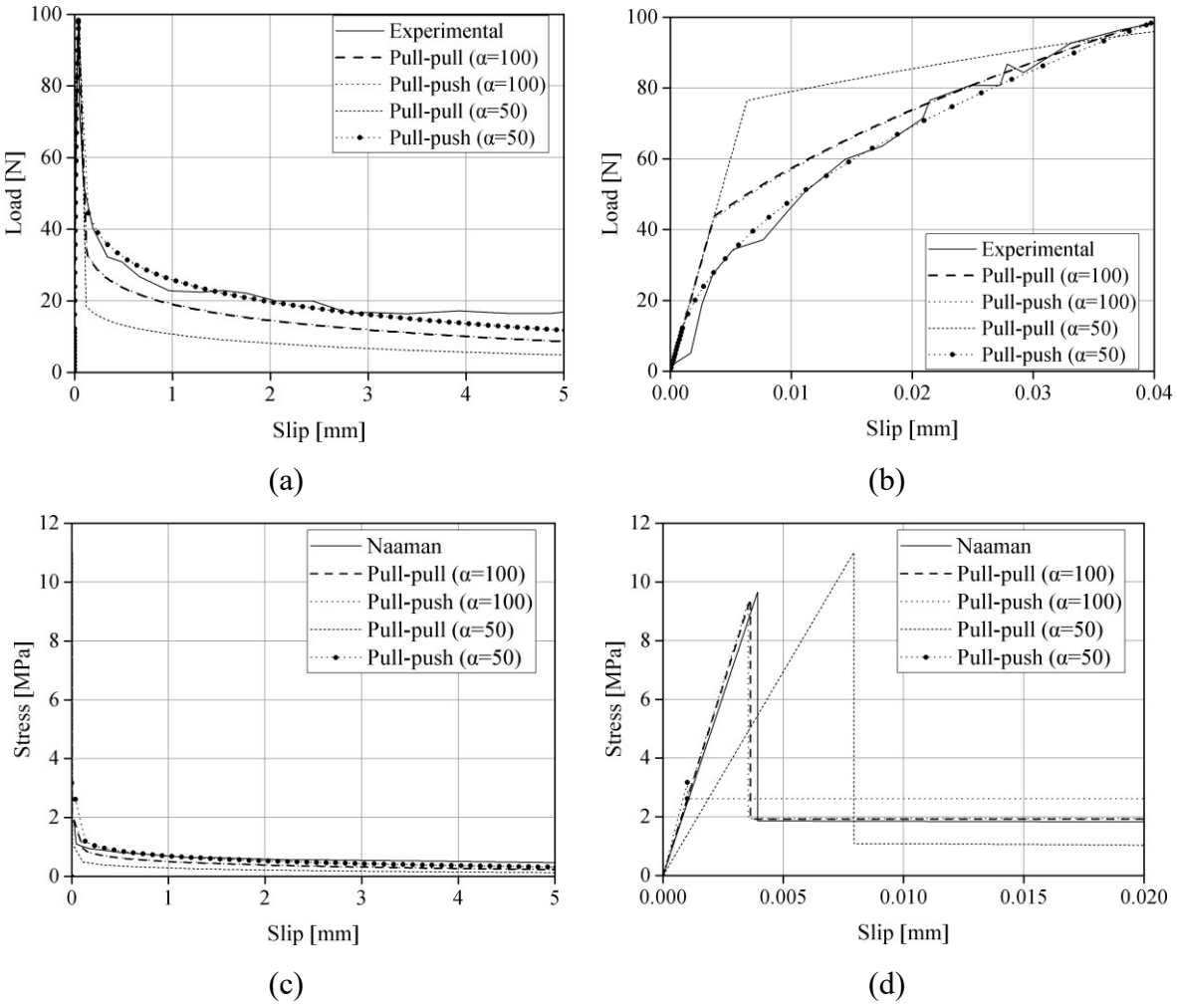

Fig. 15. Analytical modeling of experimental tests performed by Naaman et al. [39]: (a) full scale of load-slip curve; (b) ascending branch of the load-slip curve; (c) full scale of bond-slip curve; (d) enlarge scale of bond-slip curve.

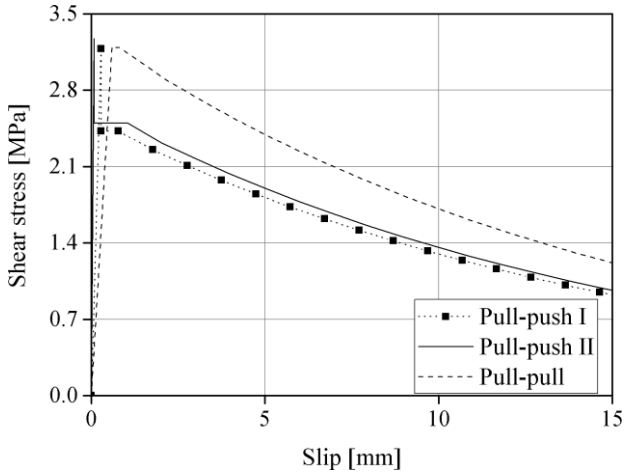

(a)

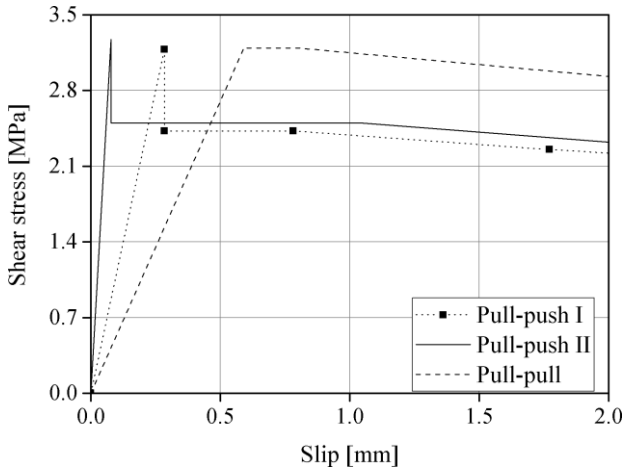

(b)

Fig. 16. Bond-slip law diagrams: (a) full scale; (b) enlarge scale.

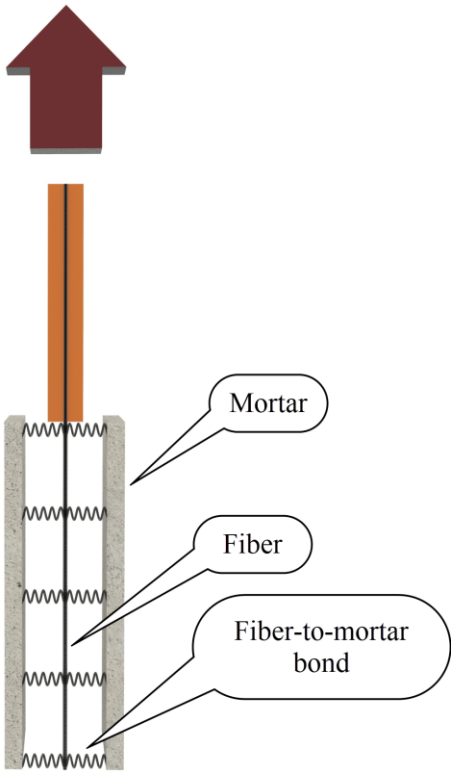

Fig. 17. Sketch of numerical modeling.

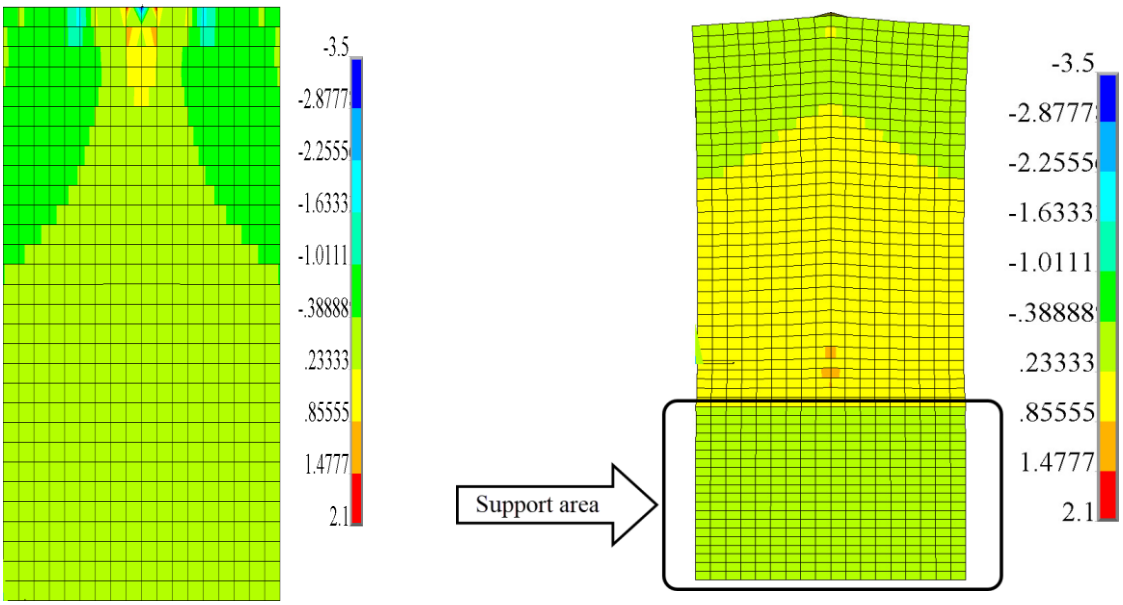

(a) (b)

Fig. 18. Stress [MPa] distribution in the mortar along the tensile applied load: (a) pull-push; (b) pull-pull.

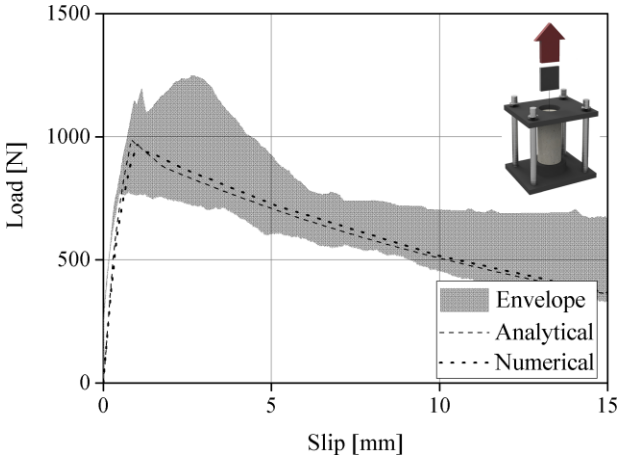

(a)

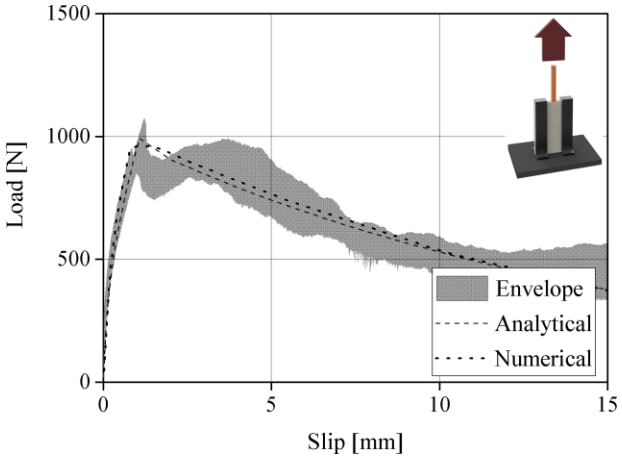

(b)

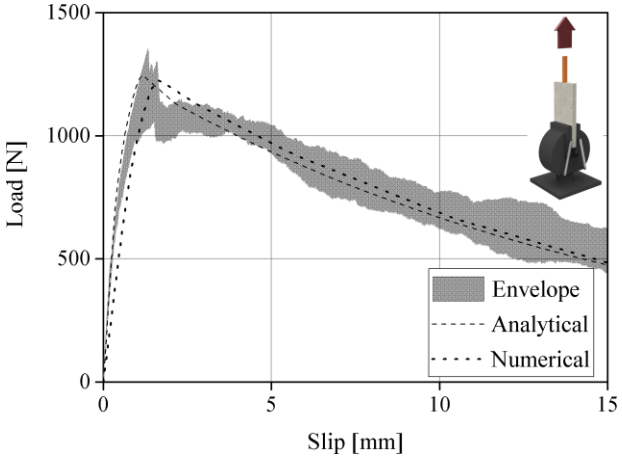

(c)

Fig. 19. Experimental pull-out curve versus analytical and numerical pull-out curve: (a) pull-push I; (b) pull-push II; (c) pull-pull.

List of Tables

Table 1. Properties of test setup specimens.

Shape of specimens	Dimensions [mm]	Test setup condition	Name of specimens
cylinder	150×75	support from top	pull-push I
disk shape	150×125×16	support from top	pull-push II
disk shape	250×125×16	support from bottom	pull-pull

Table 2. Mortar mechanical properties.

Test	3 days	7 days	14 days	28 days	60 days	90 days
compressive strength [MPa]	3.88 (8.5)	6.46 (7.8)	8.76 (7.8)	9.53 (11.1)	8.81 (13.8)	8.89 (5.9)
flexural strength [MPa]	1.4 (3.3)	1.53 (4.0)	1.79 (13.5)	2.54 (9.6)	2.09 (8.3)	2.33 (10.6)

Coefficients of variation in percentage terms are provided inside parentheses.

Table 3. Effect of test setup on the pull-out tests results.

Specimen	Slip corresponding to peak load [mm]	Peak load [N]	Toughness until peak load [N.mm]	Initial stiffness [N/mm]
pull-push I	0.78 (40.7)	987 (21.8)	571 (56.5)	1762 (9.9)
pull-push II	1.08 (17.6)	992 (9.8)	730 (23.2)	2772 (18.2)
pull-pull	1.33 (20.8)	1245 (12.5)	1098 (30.8)	2032 (27.3)

Coefficients of variation in percentage terms are provided inside parentheses.

Table 4. Bond-slip parameters for each test setup.

Specimen	P/S [N/mm]	P_P [N]	S_P [mm]	λ	κ [N/mm^3]	τ_f [N/mm^2]	$\tau_{max.}$ [N/mm^2]	S_0 [mm]
pull-push I	1762	987	0.78	0.0163	9.252	2.424	3.18	0.782
pull-push II	2772	992	1.08	0.0394	41.777	2.499	3.27	1.045
pull-pull	2032	1245	1.33	0.0133	5.408	3.192	3.2	0.804

Table 5. Comparison between analytical and numerical results.

Modeling	Specimen	Slip corresponding to peak load [mm]	Peak load [N]	Toughness until peak load [N.mm]	Initial stiffness [N/mm]
analytical	pull-push I	0.84	986	501	1758
	pull-push II	1.08	992	694	2772
	pull-pull	1.18	1245	1001	2032
numerical	pull-push I	1.0	969	611	1688
	pull-push II	1.0	961	677	2301
	pull-pull	1.6	1228	1208	1103